

# 1) Digitally controlled analog proportional-integral-derivative (PID) controller for high-speed scanning probe microscopy

Maja Dukic,<sup>1</sup> Vencislav Todorov,<sup>2</sup> Santiago Andany,<sup>1</sup> Adrian P. Nievergelt,<sup>1</sup> Chen Yang,<sup>1</sup> Nahid Hosseini,<sup>1</sup> and Georg E. Fantner<sup>1,a)</sup>

<sup>1</sup>Laboratory for Bio- and Nano-Instrumentation, School of Engineering, Ecole Polytechnique Federale de Lausanne, Lausanne 1015, Switzerland

<sup>2</sup>Techproject EMC GmbH, Vienna 1230, Austria

a) georg.fantner@epfl.ch

## Abstract

Nearly all scanning probe microscopes (SPMs) contain a feedback controller, which is used to move the scanner in direction of the z-axis in order to maintain a constant setpoint based on the tip-sample interaction. The most frequently used feedback controller in SPM is the proportional-integral (PI) controller. The bandwidth of the PI controller presents one of the speed limiting factors in high-speed SPM, where higher bandwidths enable faster scanning speeds and higher imaging resolution. Most SPM systems use digital signal processor based PI feedback controllers, which require analog-to-digital and digital-to-analog converters. These converters introduce additional feedback delays which limit the achievable imaging speed and resolution. In this paper we present a digitally controlled analog proportional-integral-derivative (PID) controller. The controller implementation allows tunability of the PID gains over a large amplification and frequency range, while also providing precise control of the system and reproducibility of the gain parameters. By using the analog PID controller, we were able to perform successful atomic force microscopy imaging of a standard silicon calibration grating at line rates up to several kHz.

## Keywords

PID, controller, AFM, SPM, analog electronics, high-speed AFM, high-speed SPM

## I. INTRODUCTION

Atomic force microscopy (AFM), a type of scanning probe microscopy (SPM), is one of the few techniques that enables us to inspect dynamics of processes on the micrometer to nanometer scale<sup>1,2</sup>. In recent years, high-speed AFM (HS-AFM) has developed into an active research area, allowing for observation of dynamic processes over short timescales<sup>1,3-7</sup>. HS-AFM was made possible by increasing the mechanical and electrical bandwidths of each of the individual components of the AFM system, such as the cantilever<sup>8-10</sup>, the scanner<sup>11-17</sup> and feedback electronic components<sup>11,13,18</sup>. Most AFM systems contain a feedback controller, which controls the scanner movement in the z-direction in order to keep the deflection or amplitude of the cantilever constant during scanning. This is usually used in order to maintain a constant force between the cantilever tip and the sample, which prevents damaging the tip

43 and the sample. The most frequently used feedback controllers in AFM are the proportional-  
44 integral (PI) and the proportional-integral-derivative (PID) controller. The bandwidth of the  
45 feedback controller is one of the limiting factors in HS-AFM and in general in SPM, where  
46 higher bandwidths enable faster scanning speeds and higher resolution.

47 Most AFM systems use digital signal processor (DSP) based PI feedback controllers. In such  
48 digital implementation of the controller, the signal needs to be sampled and afterwards  
49 quantized by an analog-to-digital converter (ADC) before it is sent to the processor. In order  
50 to avoid aliasing of high-frequency signals, it is necessary to perform signal sampling at a  
51 frequency which is usually 10 to 20 times higher than the system's closed-loop bandwidth.  
52 Additionally, the signal should be low-pass filtered before sampling, by an anti-aliasing filter  
53 to further reduce aliasing. Once the digital processor has calculated the new control value,  
54 which in turn causes an additional delay, this value needs to be converted back into a voltage  
55 by a digital-to-analog converter (DAC) in order for it to be applied to the plant (z-scanner).

56 As such, all of ADCs, DACs and filters introduce additional delays in the AFM feedback loop  
57 that limit AFM scanning speed. Moreover, ADCs and DACs can introduce quantization noise,  
58 which can be reduced by using high precision converters. As a consequence, HS-AFMs would  
59 necessitate high performance ADCs, DACs and DSPs in order to provide high speed, low noise  
60 and high conversion precision<sup>19</sup>. These parameters increase cost, power consumption and the  
61 complexity of a controller. Nevertheless, even high performance digital PI/PID controllers  
62 provide a limited bandwidth. For instance, commercial AFM PI controllers usually have a  
63 bandwidth of just a few tens of kHz, which is not sufficient for HS-AFM imaging. The reason  
64 for this is that, while ADCs and DACs can reach giga-sampling rates, they still introduce the  
65 considerable amount of delay. Recently, the increased availability of field programmable gate  
66 arrays (FPGA) has led to their use in the implementation of various parts of AFM systems,  
67 including the PID controller<sup>20</sup>. Nevertheless, they suffer from the similar problems as their  
68 DSP based counterparts. Many other control approaches were also implemented, such as H-  
69  $\infty$  controllers<sup>21-23</sup> along with various other algorithms of modern control theory<sup>24-27</sup>.  
70 However, such approaches generally lead to an increased complexity of the system and often  
71 do not allow for user input to fine-tune the control parameters optimally for each sample.

72 Compared to the digital implementation, analog PID controllers provide higher feedback loop  
73 bandwidth in their basic configuration while also eliminating noise issues present in digital  
74 implementations. As analog systems by their nature do not sample, the limitations on the  
75 bandwidth of the analog PID controller are far less restrictive. In the past years, advances in  
76 the realization of reconfigurable analog blocks led to field programmable analog array (FPAA)  
77 systems being used to successfully implement PID controllers for control of various physical  
78 processes<sup>19,28</sup> and for various control applications in AFM<sup>17,29,30</sup>. FPAA manufacturers even  
79 offer manually tunable PID control interfaces<sup>31</sup>. However, FPAAs use switched-capacitor  
80 circuits for feedback and are still quantised in time.

81 Analog PID controllers have already been successfully used in several high-speed AFM  
82 experiments. Kodera et al. state that they measured maximum 70 kHz AFM feedback  
83 bandwidth using their analog dynamic PID controller<sup>32</sup>. Schitter et al. used an analog PID  
84 controller with manual analog potentiometers for AFM imaging where they report an AFM  
85 feedback bandwidth of around 100 kHz.<sup>14</sup> Using a feed-forward approach Uchihashi et al.  
86 state that they measured 50 – 70 kHz AFM feedback bandwidth, depending on the amplitude  
87 setpoint. Although using analog PID controllers is advantageous for tracking bandwidth, the  
88 main disadvantage of the solely analog implementation of the controller is its lack of precise  
89 control and parameter reproducibility. In this work we present a digitally controllable, analog  
90 PID controller which allows precise, reproducible control of the system, as well as allows for  
91 dynamic control of the PID parameters.

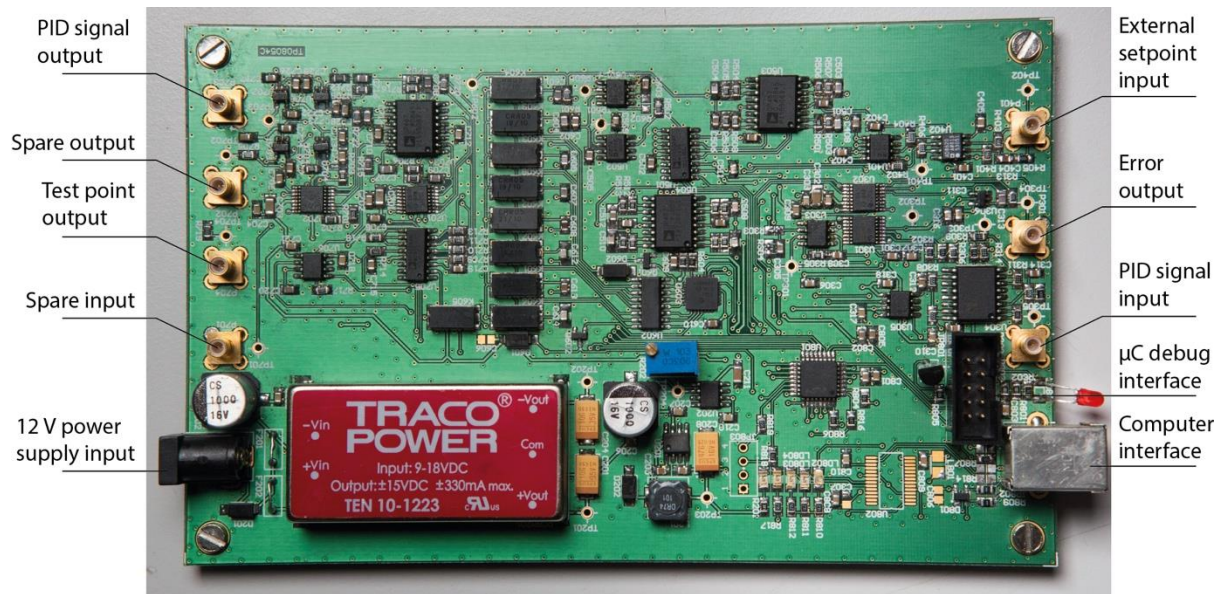
92 Combining digital control of the gain parameters with an analog controller design can provide  
93 a very precise and fast response controller. Ugodzinski et al.<sup>33</sup> developed a prototype of an  
94 analog PID controller where the digitally controlled parameters are set using compact digital  
95 potentiometers. While the device is characterized with electrical input, no bandwidth  
96 measurements are presented and the controller is not applied to controlling a plant. A  
97 commercial digitally controlled analog PID is available from Stanford Research Systems  
98 (SIM960) with a specified bandwidth of 100kHz.

99 In this paper, we present a high-speed digitally controlled analog PID controller which  
100 combines the best features from both the analog and the digital implementation. The  
101 controller allows tunability of the PID gains over a large frequency range, while also providing  
102 precise control of the system and reproducibility of the gain parameters. The precise gain  
103 control over a large gain and frequency bandwidth is an important feature of SPM feedback  
104 controller as feedback loop conditions can change dramatically from one experiment to  
105 another. By using our analog PID controller we were able to perform successful AFM imaging  
106 of a standard silicon calibration grating at line rates up to several kHz.

## 107 **II. PID CONTROLLER IMPLEMENTATION**

108 Proportional, integral and derivative parts of the system, together with summation of their  
109 outputs, can be realized in analog electronics by using operational amplifiers and passive  
110 components, such as resistors and capacitors placed at the amplifier input and in the feedback  
111 loop<sup>33</sup>. In the design of the digitally controlled analog PID, we used this analog design.  
112 However, in order to achieve digital control of the gain parameters, some of the resistors  
113 were replaced with digital-to-analog converters. These DACs convert digital control data into  
114 a certain resistance value using a resistor ladder network. In such an implementation, the  
115 user can configure the PID controller gains as well as various other operating parameters  
116 using a computer interface. The gain values are then communicated to the PID controller  
117 through a digital interface.

118 In order to achieve a higher frequency range for the integral and the derivative gain stage,  
 119 these stages were realized as a combination of two gain stages: coarse and fine. In the coarse  
 120 gain stage, a single integrator or differentiator was chosen to set the coarse gain by choosing  
 121 one of eight capacitor values. Afterwards, the gain value is fine-tuned by the fine gain stage  
 122 through an operational amplifier with a digitally controlled resistor ladder network at the  
 123 input. An image of the PID controller board is presented in Figure 1. A schematic of the  
 124 digitally controlled analog PID controller is presented in Figure 2(a).



125  
 126 FIG. 1. An image of the PID controller electrical board explaining all input and output interfaces.

127 **A. Proportional part**

128 The proportional part has only a fine gain stage implemented (Figure 2(b)). All fine gain stages  
 129 are implemented using inverting operational amplifiers (OP467GS, Analog Devices, USA). The  
 130 fine gain is tuned by changing the value of the amplifier's input resistor, which is done through  
 131 a digitally controlled R-2R resistor ladder network (DAC8812, Texas Instruments, USA). The  
 132 proportional gain can be tuned up to a gain of 1. The system response of the proportional  
 133 gain stage at maximum gain setting has a -3 dB bandwidth of about 2 MHz.

134 **B. Integral part**

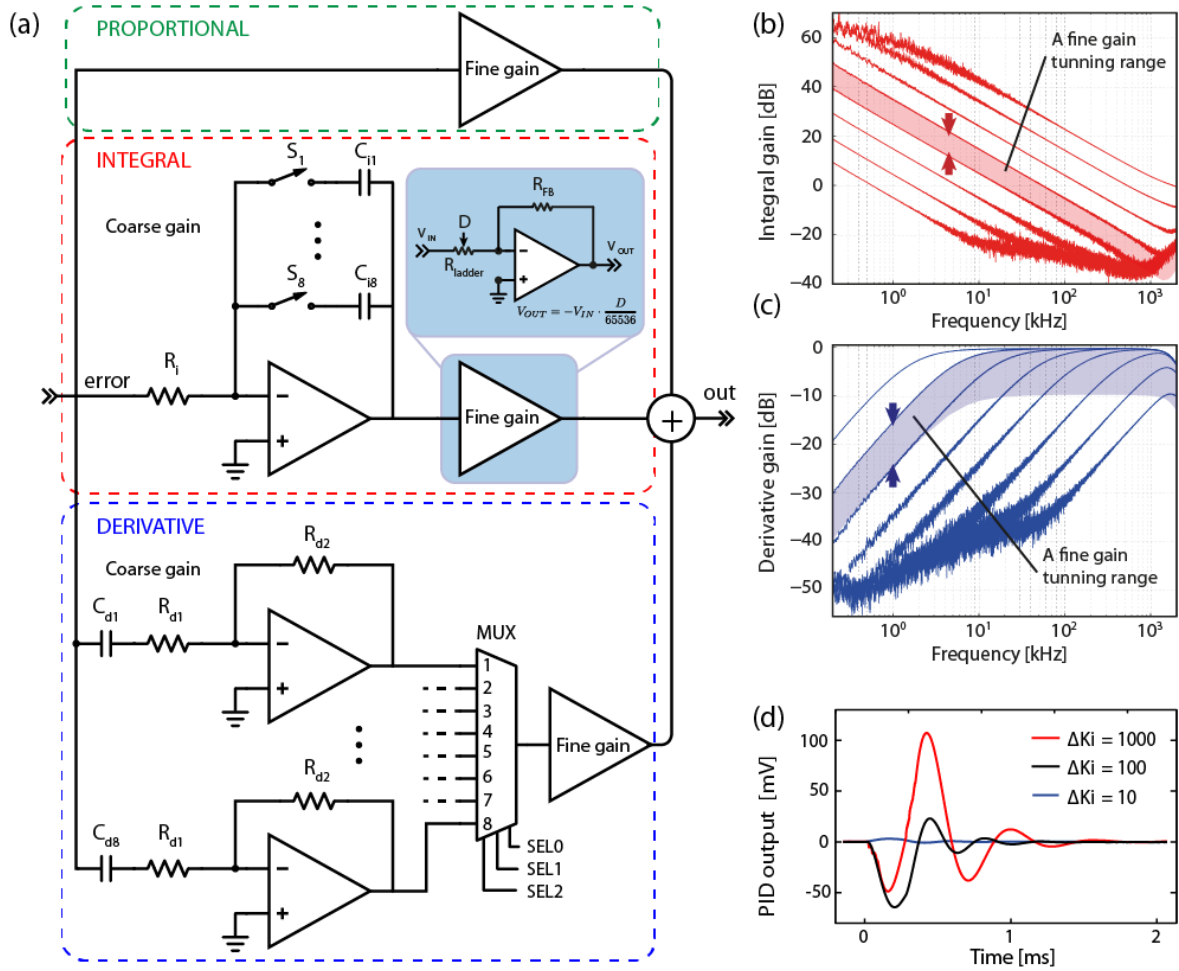
135 The coarse gain of the integral part is defined by an operational amplifier integrator (AD811JR,  
 136 Analog Devices, USA). The coarse integrator gain is set by choosing the value of the capacitor  
 137 in the feedback loop. Only one feedback capacitor is closing the feedback at a given time,  
 138 which is set by an array of reed relay switches (CRR05-1A, Meder electronic Inc, USA), as  
 139 shown in Figure 2(a). This implementation of the integral part was chosen rather than  
 140 implementing an array of operational amplifier integrators, in order to prevent overheating  
 141 of the faster integrators in saturation. The system responses of the 8 coarse integrator gain  
 142 stages are presented in Figure 2(c). The shaded area roughly represents a fine tuning range

143 of gains for a selected coarse integrator stage. The noise present in the upper gain range of  
144 the integrator characteristics comes from the closed-loop measurement procedure. The  
145 characteristics were calculated by simultaneously measuring both the input and the output  
146 of each integrator. For the faster integrators, feedback input error at lower frequencies was  
147 on par with the lock-in noise.

### 148 *C. Derivative part*

149 Saturation is not an issue in operational amplifier differentiators. For this reason, the coarse  
150 gain of the derivative part is implemented as an array of 8 operational amplifier  
151 differentiators (OP467GS, Analog Devices, USA), each one having a different time constant  
152 set by a different capacitor value at the input. Further, the coarse gain is set by selecting the  
153 output of the chosen differentiator with an analog multiplexer (ADG508, Analog Devices,  
154 USA), as presented in Figure 2(a). The system responses of the 8 coarse differentiator gain  
155 stages are presented in Figure 2(d). Again, the shaded area roughly represents a fine tuning  
156 range of gains for a selected coarse differentiator stage. Due to the fact that the gain of a  
157 derivative part increases with frequency, an additional resistor is placed at the differentiator  
158 amplifier's input to limit the gain at higher frequencies and hence limit a potential  
159 amplification of high frequency noise.

160



161

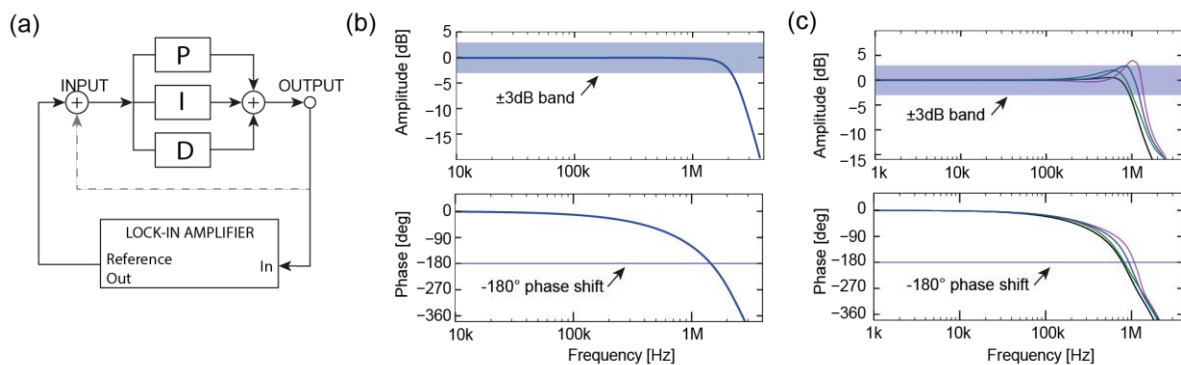
162 FIG. 2. (a) A schematic of the PID controller design, presenting the coarse and fine gain stages. The fine gain  
 163 stage is realised using a digitally controlled R-2R resistor ladder network and an inverting operational amplifier.  
 164 The value of the input resistor, and hence the amplification, is controlled by the 16-bit digital data  $D$ , according  
 165 to the equation presented in the figure. (b) Measured responses of the 8 integrator coarse gain stages. The  
 166 shaded area roughly represents a fine tuning range of gains, for a selected coarse integrator stage, with response  
 167 characteristic just above the shaded area. (c) Measured responses of the 8 differentiator coarse gain stages. The  
 168 shaded area roughly represents a fine tuning range of gains for a selected coarse differentiator stage, with  
 169 response characteristic just above the shaded area. (d) Measured transient voltage resulting from fine and  
 170 coarse integral gain changes.

171 *D. PID gain adjustment*

172 In standard AFM imaging, gains of the PID controller differ for each imaging experiment and  
 173 need to be tuned each time. It is a common routine to start imaging and then increase each  
 174 gain until visible oscillations in the feedback loop occur. Each gain is then set to the maximum  
 175 value at which no oscillations are visible. As it would be impractical to separately adjust coarse  
 176 and fine gains during PID operation, continuous integral and derivative gain adjustment was  
 177 implemented in the software (LabView, National Instruments, USA). Both gains are  
 178 exponentially increased, such as to provide the fine gain steps at lower gain values and the  
 179 large gain steps at higher gain values.

180 **III. PID CONTROLLER PERFORMANCE CHARACTERIZATION**

181 We characterized our PID controller in terms of electrical bandwidth, output noise and the  
 182 disturbance rejection sensitivity when the PID controller is placed in an AFM feedback loop.  
 183 The electrical bandwidth was measured both in open loop (P gain only), Figure 3(c), and in  
 184 closed loop by sweeping the frequency of the input signal, while the PID output was fed back  
 185 to the external setpoint input (Figure 3(c)). The gains of the PID controller were increased up  
 186 to the point where frequency response peaking would start to show and several curves with  
 187 different gain settings were measured. The amplitude and the phase frequency response of the  
 188 PID controller, measured under such set gains, are presented in Figure 3(b). The  $-3$  dB  
 189 bandwidth was measured to be about 834 kHz.



190  
 191 FIG. 3. Electrical bandwidth measurement: (a) A schematic of the measurement setup. Dotted line was  
 192 connected for closed loop measurement in panel c. (b) Open loop transfer function of the PID with the I and D  
 193 gains set to zero. The phase drops to 180deg at ca 1.5MHz.(c) Closed loop frequency response of the PID  
 194 without a plant, showing increasing peaking and higher bandwidth for higher gain settings.

195 It should be noted from the open loop phase response (see Figure 3(b)) that the phase loss  
 196 reaches  $-180^\circ$  at 1.5MHz, which will limit the closed loop bandwidth (Figure 3(c)). The reason  
 197 for this is that the current implementation has a large array of operational amplifiers and  
 198 switches on the signal path, each of them contributing a certain phase delay. This design was  
 199 implemented in order to provide more options for testing the circuit as well as various  
 200 functionalities such as an inversion of the input signal, amplification of an error signal and the  
 201 option to switch off individual gain parts. Simplifying the design of the system by removing  
 202 some of these options, and therefore decreasing the number of components, would lead to  
 203 a reduction of the phase loss and a to a better overall performance of the controller.

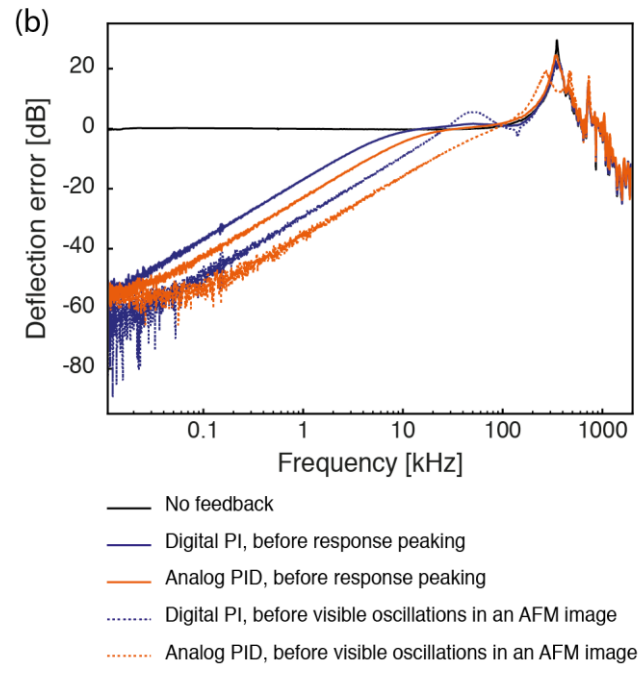
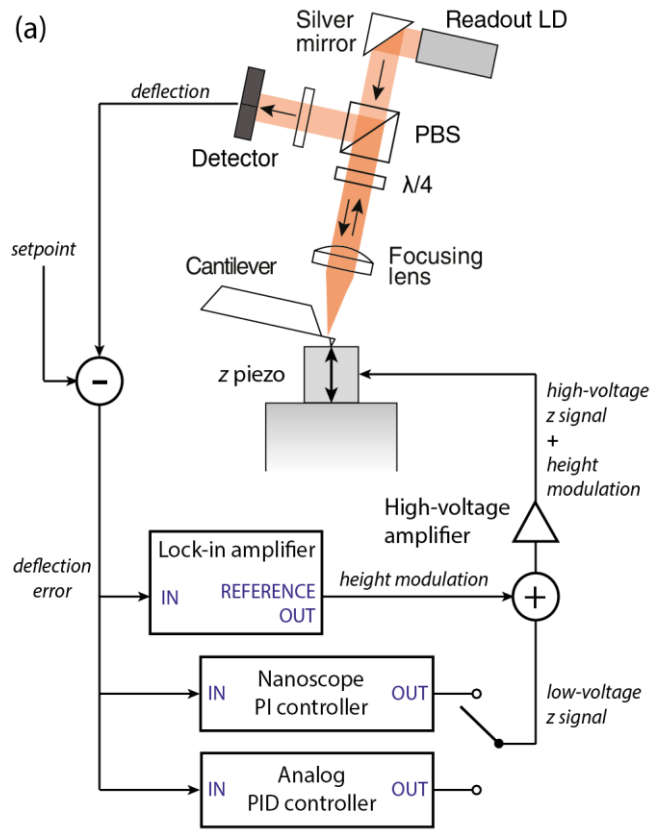
204 We also measured the voltage noise spectral density on the PID controller output. The PID  
 205 controller was connected as shown in Figure 3(a), and gains were increased just up to the  
 206 point where the frequency response peaking would start to show. The input of the PID  
 207 controller was terminated with a  $50 \Omega$  resistance and the setpoint was set to 0 V. Output noise  
 208 level of the base line above 100 Hz was typically around  $0.2 - 0.4 \mu\text{V}/\sqrt{\text{Hz}}$ . However, some  
 209 noise spurs were also present during the measurement. These spurs could be a result of the  
 210 measurement, the DC/DC converter, or residual crosstalk from the digital logic controlling the  
 211 R-2R networks..

212 We tested the performance of our analog PID controller and that of commercial FPGA-based  
213 high-speed controllers (Nanoscope V & Nanoscope 3A, Bruker) in an AFM feedback loop  
214 (Multimode 8 AFM, Bruker). We measured the disturbance rejection of the PID controller in  
215 an AFM feedback loop. We performed a comparison between our analog PID controller and  
216 the digital controller present in the standard commercial AFM system, see Figure 4. A  
217 sinusoidal height modulation (disturbance) at variable frequency was added to the z-axis  
218 controller output and the resulting deflection of the cantilever in contact mode was measured  
219 (see Figure 4(a) for measurement setup). A custom made fast z-scanner with a flat response  
220 up to around 200 kHz, a custom made high-speed high-voltage piezo amplifier<sup>34</sup> and a  
221 custom-built AFM head<sup>35,36</sup> were used in the measurements. The gains of both PID controllers  
222 were increased up to the point where visible oscillations of the system would start to show in  
223 the AFM image or up the point where there was no visible frequency response peaking  
224 present in the closed-loop response. Figure 4(b) shows the disturbance rejection sensitivity  
225 for both cases. The disturbance rejection sensitivity is a measurement of the residual error  
226 when the controller tracks topography changes at different frequencies.

227 With increasing frequency of the disturbance, the PID controller will stop reacting fast enough  
228 to produce an appropriate signal to cancel the cantilever deflection error. At that point, the  
229 cantilever deflection error starts to rise. Finally, past a certain frequency, the PID controller  
230 will not track the surface at all and the entire height disturbance will be present in the  
231 cantilever deflection error. From Figure 4(b) we see that the analog PID controller rejects the  
232 height disturbances at frequencies up to one order of magnitude higher than the digital PI  
233 controller.

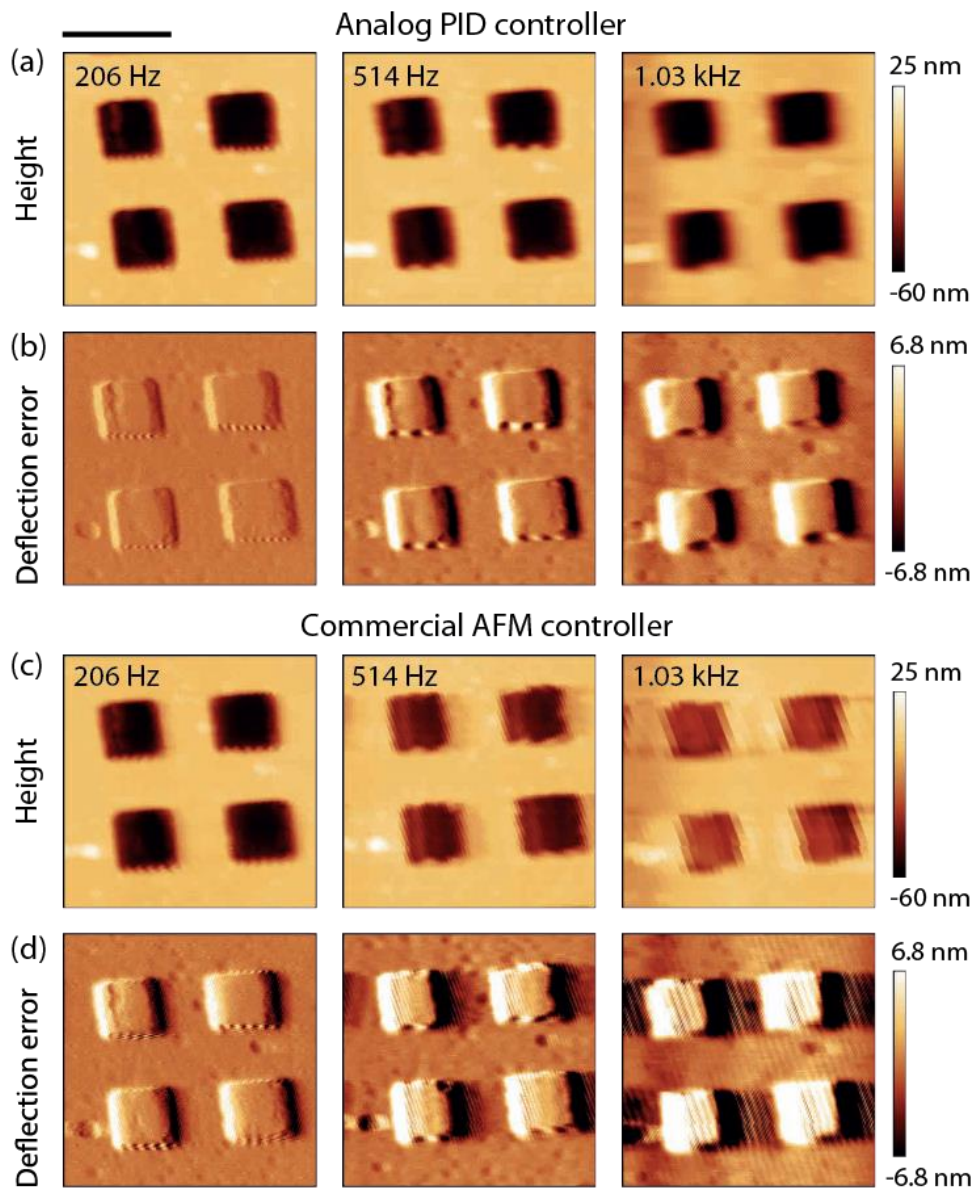
234 The resonance peak at around 300 kHz is resonance of the z-scanner. The peaking in the  
235 response measured just before visible oscillations in an AFM image occur (dashed lines in  
236 Figure 4.) comes from the fact that we increased the gains to the point where the system  
237 becomes unstable. The frequency of the peaks, and hence the bandwidth of the closed-loop  
238 feedback is determined by the combined delays of various components in the AFM feedback  
239 loop: scanner, deflection readout, PID controller and high-voltage amplifier.





240  
241  
242  
243  
244  
245  
246  
247

FIG. 4. Comparison of the closed loop disturbance rejection sensitivity between the presented analog PID and the standard commercial digital controller in cantilever surface tracking: (a) Measurement setup. (b) The measured disturbance rejection sensitivity measures the ability of the controller to track topographic changes at different frequencies. The proposed analog PID controller (red) is almost an order of magnitude faster than the commercial digital PI controller (blue) for the same measurement conditions.



249

250 FIG. 5. A comparison of HS-AFM imaging between the analog PID and the standard commercial digital controller.  
 251 a) The tracking performance of the analog PID decreases with increasing line rate, but the pits of the calibration  
 252 standard are still clearly resolved in depth when scanning at 1030 lines/s. b) The deflection error image shows  
 253 IV. that the controller manages to descend into the pits reproducibly and quickly. c) In comparison to the analog  
 254 PID, the commercial digital controller quickly degrades in tracking performance and shows noticeable  
 255 quantisation artifacts. d) Even at 514 lines/s the commercial controller does not manage to descend into the pits  
 256 anymore, and at 1030 lines/s the tracking degrades enough that the height of the pits is severely distorted.

## 257 V. HIGH-SPEED AFM IMAGING PERFORMANCE

258

259 We used the analog PID controller to perform HS-AFM imaging in contact mode, using a soft  
 260 cantilever probe in air (spring constant of 0.4N/m and resonance frequency of 70kHz). The  
 261 imaging was performed with a custom made AFM high-speed scanner, similar to the one  
 262 published in<sup>13,14</sup> and a custom-built AFM head<sup>37</sup>. The AFM image acquisition was performed  
 263 with a custom made data acquisition system<sup>13,38</sup>. We used a commercial high-speed AFM

264 piezoamplifier (Techproject EMC, Austria) for driving the slow axis piezos of the scanner. For  
265 driving the fast axis and the z-piezo, a custom made high-speed high-voltage piezo amplifier  
266 was used<sup>39</sup>. We used a silicon calibration grating ( $1\ \mu\text{m} \times 1\ \mu\text{m}$ , 50 nm deep) as a sample to  
267 test the HS-AFM imaging performance of the analog PID controller.

268 Figure 5. shows a comparison of HS-AFM images obtained using the analog PID controller and  
269 the digital controller present in the standard commercial AFM. The images were taken at 206  
270 Hz, 514 Hz and 1.03 kHz line rates. For both controllers, the gains were set just below the  
271 point where oscillations in the feedback loop would appear. From the deflection error images,  
272 one can notice that the analog PID was tracking the sample surface significantly better at all  
273 speeds. The commercial AFM PI controller is also limited in the sampling speed of its analog-  
274 to-digital and digital-to-analog converters, which makes images look increasingly pixelated at  
275 higher scanning speeds. The sampling rate of the commercial PI was measured to be around  
276 60 kHz.

277 During AFM imaging, the gains need to be often adjusted to obtain an optimal AFM image. In  
278 our digitally controlled analog PID, small gain changes (changes in the R-2R ladder) result in  
279 only minor transients which settle down quickly during imaging. Larger changes (switching  
280 gain ranges) however cause moderately high transients. Even in the worse switching  
281 configurations (coarse integral changes), these transients do not damage the AFM tip as the  
282 amplitude of the Z-piezo perturbation they generate is well below 20nm.

283 In order to test the worst case, we performed a 1000x gain change (from  $K_i = 1$  to  $K_i = 1000$ ),  
284 including both resistor network switching as well as coarse gain switching, see the red line  
285 below. This large change did induce a significant swing in the output voltage of the PID and  
286 thus on the piezo control voltage (as is to be expected). Nevertheless, even for this extreme  
287 gain change, the output voltage swing is only about 150mV which, after amplification,  
288 corresponds to an actual displacement of the Z-piezo of less than 20nm. Fortunately, this is  
289 not sufficient to damage the AFM tip.

290 The comparison shows the potential to improve the feedback controller bandwidth if we want  
291 to reach kHz line rates. While at few 100s of Hz/s line rates a commercial digital feedback  
292 controller could still track the sample (see Figure 5, at 206 Hz and 512 Hz line rates) – at 1 kHz  
293 line rate the tracking with our existing digital controller is not possible (see Figure 5, at 1.03  
294 kHz line rates). It should be noted, however, that by using higher speed D/A converters and  
295 more powerful digital processors it would be possible to increase the feedback bandwidth as  
296 well. The efforts to increase the feedback bandwidth to the level of the analog PID, however,  
297 are significantly more than what is needed to add digital control to an analog PID.

298

299 **VI. DISCUSSION AND CONCLUSION**

300

301 Due to signal sampling and aliasing issues, digital PID controllers must operate at frequencies  
302 that are 10-20 times higher than the closed loop bandwidth of the overall control loop. On  
303 the other hand, analog controllers do not face such issues and should be able to provide much  
304 faster response. Previously, due to the lack of the possibility to adjust control parameters at  
305 run-time, analog PID controllers were mostly used in control of invariable processes, where  
306 the desired control gains were determined and set by fixed components to never or rarely  
307 change. Implementing digital control of the analog controller parameters opens up new  
308 possibilities for the use of analog PID controllers, which can be especially beneficial for the  
309 control of fast processes.

310 One of the benefits of digital controllers is that they can be easily reconfigured (e.g. to include  
311 or exclude some gain parameters or to change the PID configuration from parallel to serial  
312 etc.). In our analog PID controller, we enabled a user to include or exclude some of the PID  
313 gains by using analog switches. However, the switches introduce additional phase loss on the  
314 signal path and limit the controller bandwidth.

315 Although the derivative part of the feedback controller is usually omitted in standard AFM  
316 systems due to the fact that it amplifies high frequency noise, we performed AFM imaging  
317 with and without the derivative part (derivative gain was set to almost zero) and we found  
318 that the derivative part still helped to slightly improve the image quality and tracking.

319

320 We developed a digitally controlled analog PID controller and successfully demonstrated that  
321 it can be used in high-speed AFM imaging at several kHz line rates and several mm/s surface  
322 speed. The current design of the PID controller could be improved in terms of bandwidth and  
323 phase loss by simplifying the design and removing some of the components in the signal path,  
324 and by replacing some components for ones with a faster performance. We think that the  
325 noise of the system could also be improved by a redesign, for instance by replacing the  
326 switching DC/DC converter power supply currently being used.

327 **ACKNOWLEDGEMENTS**

328

329 This work has been funded by the European Union's Seventh Framework Programme  
330 FP7/2007-2011 under grant 286146, by the European Union FP7/2007-2013/ERC under Grant  
331 Agreement No. 307338-NaMic, and Eurostars Eurostars E!8213-TripleS. C.Y. acknowledges  
332 the financial support from the China Scholarship Council for his joint PhD project (Grant  
333 No.201306120115).

334

335 <sup>1</sup> A.J. Katan and C. Dekker, *Cell* **147**, 979 (2011).

336 <sup>2</sup> T. Ando, *Nanotechnology* **23**, 62001 (2012).

337 <sup>3</sup> N. Kodera, D. Yamamoto, R. Ishikawa, and T. Ando, *Nature* **468**, 72 (2010).

338 <sup>4</sup> G.E. Fantner, R.J. Barbero, D.S. Gray, and A.M. Belcher, *Nat. Nanotechnol.* **5**, 280 (2010).

339 <sup>5</sup> I. Casuso, P. Sens, F. Rico, and S. Scheuring, *Biophys. J.* **99**, L47 (2010).

340 <sup>6</sup> T. Uchihashi, R. Iino, T. Ando, and H. Noji, *Science* **333**, 755 (2011).

341 <sup>7</sup> M. Imamura, T. Uchihashi, T. Ando, A. Leifert, U. Simon, A.D. Malay, and J.G. Heddle, *Nano*

342 *Lett.* **15**, 1331 (2015).

343 <sup>8</sup> M.B. Viani, T.E. Schäffer, A. Chand, M. Rief, H.E. Gaub, and P.K. Hansma, *J. Appl. Phys.* **86**,

344 2258 (1999).

345 <sup>9</sup> M. Kitazawa, K. Shiotani, and A. Toda, *Japanese J. Appl. Physics, Part 1 Regul. Pap. Short*

346 *Notes Rev. Pap.* **42**, 4844 (2003).

347 <sup>10</sup> J.D. Adams, B.W. Erickson, J. Grossenbacher, J. Brugger, A. Nievergelt, and G.E. Fantner,

348 *Nat. Nanotechnol.* **11**, 147 (2015).

349 <sup>11</sup> T. Ando, N. Kodera, E. Takai, D. Maruyama, K. Saito, and A. Toda, *Proc. Natl. Acad. Sci. U.*

350 *S. A.* **98**, 12468 (2001).

351 <sup>12</sup> A.D.L. Humphris, M.J. Miles, and J.K. Hobbs, *Appl. Phys. Lett.* **86**, 34106 (2005).

352 <sup>13</sup> G.E. Fantner, G. Schitter, J.H. Kindt, T. Ivanov, K. Ivanova, R. Patel, N. Holten-Andersen, J.

353 Adams, P.J. Thurner, I.W. Rangelow, and P.K. Hansma, *Ultramicroscopy* **106**, 881 (2006).

354 <sup>14</sup> G. Schitter, K.J. Astrom, B.E. DeMartini, P.J. Thurner, K.L. Turner, and P.K. Hansma, *IEEE*

355 *Trans. Control Syst. Technol.* **15**, 906 (2007).

356 <sup>15</sup> C. Braunsman and T.E. Schäffer, *Nanotechnology* **21**, 225705 (2010).

357 <sup>16</sup> A.P. Nievergelt, B.W. Erickson, N. Hosseini, J.D. Adams, and G.E. Fantner, *Sci. Rep.* **5**,

358 11987 (2015).

359 <sup>17</sup> C. Yang, J. Yan, M. Dukic, N. Hosseini, J. Zhao, and G.E. Fantner, *Scanning* **9999**, 1 (2016).

360 <sup>18</sup> B. Schlecker, M. Dukic, B. Erickson, M. Ortmanns, G. Fantner, and J. Anders, *IEEE Trans.*

361 Biomed. Circuits Syst. **8**, 206 (2014).

362 <sup>19</sup> V. Aggarwal, Meng Mao, and U.-M. O'Reilly, in *First NASA/ESA Conf. Adapt. Hardw. Syst.*  
363 (IEEE, 2006), pp. 12–19.

364 <sup>20</sup> Yifan Sun, Y. Fang, Yudong Zhang, and Xiaokun Dong, in *2010 IEEE Int. Conf. Control Appl.*  
365 (IEEE, 2010), pp. 245–250.

366 <sup>21</sup> G. Schitter, P. Menold, H.F. Knapp, F. Allgower, and A. Stemmer, *Rev. Sci. Instrum.* **72**,  
367 3320 (2001).

368 <sup>22</sup> S. Salapaka, A. Sebastian, J.P. Cleveland, and M. V. Salapaka, *Rev. Sci. Instrum.* **73**, 3232  
369 (2002).

370 <sup>23</sup> N. Chuang, in *2014 Australas. Univ. Power Eng. Conf.* (IEEE, 2014), pp. 1–6.

371 <sup>24</sup> Hiroshi Fujimoto and Takashi Oshima, in *2008 10th IEEE Int. Work. Adv. Motion Control*  
372 (IEEE, 2008), pp. 568–573.

373 <sup>25</sup> Ying Wu, Qingze Zou, and Chanmin Su, in *2008 Am. Control Conf.* (IEEE, 2008), pp. 2040–  
374 2045.

375 <sup>26</sup> U. Aridogan, Y. Shan, and K.K. Leang, *J. Dyn. Syst. Meas. Control* **131**, 61103 (2009).

376 <sup>27</sup> S. Necipoglu, S. a. Cebeci, Y.E. Has, L. Guvenc, and C. Basdogan, *IEEE Trans. Nanotechnol.*  
377 **10**, 1074 (2011).

378 <sup>28</sup> I. Lita, D.A. Visan, and I.B. Cioc, in *2009 32nd Int. Spring Semin. Electron. Technol.* (IEEE,  
379 2009), pp. 1–4.

380 <sup>29</sup> G. Schitter and N. Phan, in *2008 Am. Control Conf.* (IEEE, 2008), pp. 2690–2695.

381 <sup>30</sup> Y.K. Yong, B. Bhikkaji, and S.O.R. Reza Moheimani, *IEEE/ASME Trans. Mechatronics* **18**,  
382 1060 (2013).

383 <sup>31</sup> Anadigm, Chapter 9: AnadigmPID (2004).

384 <sup>32</sup> N. Kodera, M. Sakashita, and T. Ando, *Rev. Sci. Instrum.* **77**, 83704 (2006).

385 <sup>33</sup> R. Ugodzinski, R. Szewczyk, and M. Nowicki, *Filev D. Al. Intell. Syst. Adv. Intell. Syst.*  
386 *Comput.* **323**, 89 (2015).

387 <sup>34</sup> A.P. Nievergelt, S.H. Andany, J.D. Adams, M.T. Hannebelle, and G.E. Fantner, *IEEE/ASME*  
388 *Int. Conf. Adv. Intell. Mechatronics, AIM* **Accepted**, (2017).

389 <sup>35</sup> J.D. Adams, A. Nievergelt, B.W. Erickson, C. Yang, M. Dukic, and G.E. Fantner, *Rev. Sci.*  
390 *Instrum.* **85**, (2014).

391 <sup>36</sup> A.P. Nievergelt, J.D. Adams, P.D. Odermatt, and G.E. Fantner, *Beilstein J. Nanotechnol.* **5**,  
392 2459 (2014).

393 <sup>37</sup> J.D. Adams, C.H. Schwalb, M. Winhold, M. Đukić, M. Huth, and G.E. Fantner, *Proc. SPIE*  
394 *Microtechnologies, Smart Sensors, Actuators, MEMS* **8763**, 876327 (2013).

395 <sup>38</sup> G.E. Fantner, P. Hegarty, J.J.H. Kindt, G. Schitter, G.A.G. Cidade, and P.K. Hansma, *Rev. Sci.*  
396 *Instrum.* **76**, 26118 (2005).

397 <sup>39</sup> S. Andany, A.P. Nievergelt, M. Dukic, and G.E. Fantner, in *Int. Scanning Probe Microsc.*  
398 *Conf.* (Grindelwald, 2016).

399